Möbius-invariant curve and surface energies and their applications

Shin YOSHIZAWA[1] and Alexander BELYAEV[2]
[1]Image Processing Research Team, RIKEN, Japan, shin@riken.jp
[2]Institute of Sensors, Signals & Systems, Heriot-Watt University, UK, a.belyaev@hw.ac.uk

Abstract:
Curvature-based surface energies are frequently used in mathematics, physics, thin plate and shell engineering, and membrane chemistry and biology studies. Invariance under rotations and shifts makes curvature-based energies very attractive for modeling various phenomena. In computer-aided geometric design, the Willmore surfaces and the so-called minimum variation surfaces (MVS) are widely used for shape modeling purposes. The Willmore surfaces are invariant w.r.t conformal transformations (Möbius or conformal invariance), and studied thoroughly in differential geometry and related disciplines. In contrast, the minimum variation surfaces are not conformal invariant. In this paper, we suggest a simple modification of the minimum variation energy and demonstrate that the resulting modified MVS enjoy Möbius invariance (so we call them conformal-invariant MVS or, shortly, CI-MVS). We also study connections of CI-MVS with the cyclides of Dupin. In addition, we consider several other conformal-invariant curve and surface energies involving curvatures and curvature derivatives. In particular, we show how filtering with a conformal-invariant curve energy can be used for detecting salient subsets of the principal curvature extremum curves used by Hosaka and co-workers for shape quality inspection purposes.

Keywords: Willmore energy, minimum variation surfaces, Dupin's cyclides, Möbius/conformal invariance.

1 Introduction

The so-called Bernoulli-Euler's *elastica* curves were first considered by Bernolli at the end of the 17th century in relation to a mechanical equilibrium problem for elastically bending shapes. Later, Euler introduced a curvature-based formulation of elastica [5] and considered a curvature-based energy $\int k^2\, ds$, where k and ds are the curvature and arc length element of a curve, respectively. Since then the elastica and related curvature-based curve and surface energies have been widely studied in mathematics, physics, engineering, computer vision, biochemistry, architecture, and other disciplines. See [13] for a historical survey of the elastica.

A natural extension of the elastica to surfaces is given by the well-known Willmore surfaces [28, 29] which minimize the elastic bending energy (Willmore energy)

$$\int\!\!\int (k_{\max}^2 + k_{\min}^2)\, dA \tag{1}$$

where $k_{\max}$, $k_{\min}$, and dA are the principal curvatures and area element of a surface, respectively. We assume that $k_{\min} \le k_{\max}$. The Willmore surfaces possess beautiful mathematical properties. In particular, they are invariant under conformal transformations: the so-called Möbius invariance [27] and studied thoroughly in differential geometry [10] and related mathematical disciplines [7, 9, 3, 21, 15]. The Willmore energy (1) measures a deviation from sphericity and is currently a subject of intensive researches in geometric modeling [2, 24]; see also references therein.

Moreton and Séquin introduced the so-called minimum variation curves (MVC) [18] and surfaces (MVS) [19] which bend shapes as smoothly as possible, where the bending smoothness is modeled by the variation of curvatures, minimizing the MVC energy $\int (dk/ds)^2 ds$ and MVS energy

$$\int\!\!\int (e_{\max}^2 + e_{\min}^2)\, dA \tag{2}$$

where $e_{\max} = \partial k_{\max}/\partial \mathbf{t}_{\max}$ and $e_{\min} = \partial k_{\min}/\partial \mathbf{t}_{\min}$ are the first order principal curvature derivatives w.r.t. their corresponding principal directions $\mathbf{t}_{\max}$ and $\mathbf{t}_{\min}$. The MVC and MVS energies measure the magnitude of the rate of change of curvatures, and provide more aesthetic shapes than the Willmore surfaces. The MVS energy (2) also measures deviation from special surfaces called Dupin's *cyclides* (see Figure 1) which are characterized by the conditions $e_{\max} = 0 = e_{\min}$ and which are often used as CAD primitives.

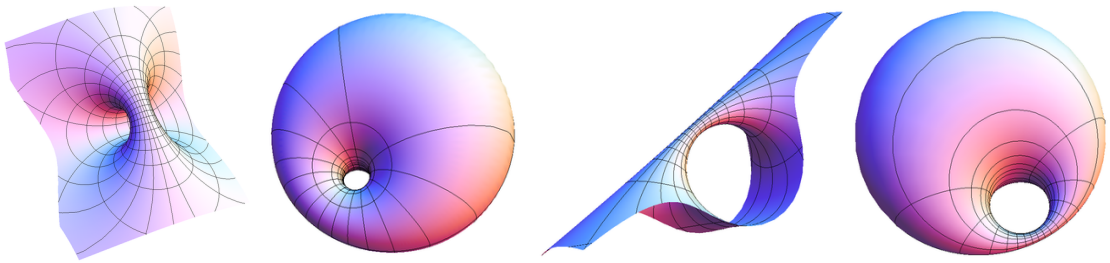

Figure 1: Examples of Dupin cyclides.

Various modifications of the MVC energy were considered in [12] including

$$\iint [e_{\max}^2 + (\frac{\partial k_{\max}}{\partial \mathbf{t}_{\min}})^2 + e_{\min}^2 + (\frac{\partial k_{\min}}{\partial \mathbf{t}_{\max}})^2]\, dA \cdot \iint dA \quad (3)$$

where the factor $\iint dA$ is used to maintain the scale-invariance.

Unfortunately, MVS, their modifications as those from [12] and other high-order curvature-based energies used for shape modeling applications (e.g. $\iint |\nabla H|^2\, dA$ [30] where ∇H is the surface gradient of the mean curvature) are not conformal invariant.

In this paper[1], we introduce a novel conformal-invariant surface energy (4) which we call the conformal-invariant MVC (CI-MVC) energy. We also study connections of CI-MVS with the cyclides and curvature-based surface creases which also enjoy conformal invariance. In particular, efficient filtering the surface creases with a conformal-invariant curve energy is demonstrated. All numerical experiments in this paper are performed on surfaces approximated by dense triangle meshes.

2 Conformal Invariant MVS Energy

The conformal invariant minimum variation surfaces (CI-MVS) are the minimizers of the energy functional

$$\iint \sqrt{e_{\max}^2 + e_{\min}^2}\, dA \quad (4)$$

where a conformal-invariant energy remains unchanged under the conformal transformations consisting of translations, rotations, scaling, and spherical inversions. Conformal transformations have been employed in many CG and CAD applications e.g. geometric algebra [14], pose and motion estimations [25], and surface classification [8]. In addition, spherical inversions are also useful for geometric computing tasks such as visibility computation of point set surfaces [16] and chord length parameterization of Bézier surfaces [1]. See also Section 3 where we discuss why invariance under conformal transformations (instead of only rigid motions) is important in aesthetic shape design.

Proof for conformal invariance of (4). The principal curvatures and directions ($k_{\max}$, $k_{\min}$, $\mathbf{t}_{\max}$, and $\mathbf{t}_{\min}$) are obviously invariant under any rigid motions (translations and rotations) because they do not depend on any surface parameterization and choice of a coordinate system. Consequently, $e_{\max}$ and $e_{\min}$ are also translational- and rotational-invariants. Since it is a straightforward computation, we omit the derivations of

$$k^\alpha = \frac{1}{\alpha} k, \qquad e^\alpha = \frac{1}{\alpha^2} e \quad (5)$$

where α is a constant scaling factor, $k^\alpha = k^\alpha_{\max}, k^\alpha_{\min}$ and $e^\alpha = e^\alpha_{\max}, e^\alpha_{\min}$ are the principal curvatures and their corresponding derivatives of the scaled surface $\mathbf{r}^\alpha = \alpha \mathbf{r}$ associated with $k = k_{\max}, k_{\min}$ and $e = e_{\max}, e_{\min}$, respectively. The scale invariance property is shown by

$$\iint \sqrt{(e^\alpha_{\max})^2 + (e^\alpha_{\min})^2}\, dA_\alpha = \iint \sqrt{e^2_{\max} + e^2_{\min}}\, dA$$

where $dA_\alpha = \alpha^2 dA$ is the area element of $\mathbf{r}^\alpha$. Now it remains to demonstrate the inversion invariance of (4).

2.1 Inversion Invariance

Consider a surface $\tilde{\mathbf{r}}$ obtained from $\mathbf{r}$ by the inversion w.r.t. the sphere of radius c centered at the origin of coordinates

$$\tilde{\mathbf{r}} = c^2 \mathbf{r}/r^2, \qquad r^2 = \mathbf{r} \cdot \mathbf{r}.$$

Then the length and area elements of $\tilde{\mathbf{r}}$ and $\mathbf{r}$ are related by

$$d\tilde{s} = c^2 ds / r^2, \qquad d\tilde{A} = \frac{c^4}{r^4} dA. \quad (6)$$

Direct computations (see [26, Art. 82-83] or Appendix A of this paper) show that the principal curvatures of $\tilde{\mathbf{r}}$ are given by

$$\tilde{k}_{\max} = -\frac{r^2}{c^2} k_{\min} - 2\frac{(\mathbf{r} \cdot \mathbf{n})}{c^2}, \quad (7)$$

$$\tilde{k}_{\min} = -\frac{r^2}{c^2} k_{\max} - 2\frac{(\mathbf{r} \cdot \mathbf{n})}{c^2}, \quad (8)$$

[1] It is an extension of our previous work [31]. The main difference from [31] is the numerical comparisons of the proposed and conventional energies under spherical inversions.

where $\mathbf{n}$ is a unit normal of $\mathbf{r}$ and $\tilde{k}_{\min} \le \tilde{k}_{\max}$ [26, Art. 82-83]. The curvature lines of $\mathbf{r}$ are mapped onto the curvature lines of $\tilde{\mathbf{r}}$ such that $\tilde{\mathbf{t}}_{\max} = \mathbf{t}_{\min}$ and $\tilde{\mathbf{t}}_{\min} = \mathbf{t}_{\max}$, where $\tilde{\mathbf{t}}_{\max}$ and $\tilde{\mathbf{t}}_{\min}$ are the principal directions corresponding to the principal curvatures $\tilde{k}_{\max}$ and $\tilde{k}_{\min}$, respectively.

One can easily observe that (6), (7), and (8) imply the inversion invariance of the energy

$$\iint (\tilde{k}_{\max} - \tilde{k}_{\min})^2 \, d\tilde{A}$$

corresponding to (1). Since $\iint k_{\max} k_{\min} \, dA$ becomes a constant depending only on topology of $\mathbf{r}$ from the Gauss-Bonnet theorem (see, for example, [22, p. 155]), minimizing

$$\iint (k_{\max}^2 + k_{\min}^2) \, dA - 2 \iint k_{\max} k_{\min} \, dA$$

is equivalent to minimizing (1).

Curvature Derivatives. Differentiating $\tilde{k}_{\max}$ and $\tilde{k}_{\min}$ in (7) and (8) w.r.t. the parameters v and u, respectively, gives

$$\frac{\partial \tilde{k}_{\max}}{\partial v} = -2\frac{r}{c^2}\frac{\mathbf{r}_v \cdot \mathbf{r}}{r} k_{\min} - \frac{r^2}{c^2}\frac{\partial k_{\min}}{\partial v} - 2\frac{\mathbf{r}_v \cdot \mathbf{n} + \mathbf{r} \cdot \mathbf{n}_v}{c^2},$$

$$\frac{\partial \tilde{k}_{\min}}{\partial u} = -2\frac{r}{c^2}\frac{\mathbf{r}_u \cdot \mathbf{r}}{r} k_{\max} - \frac{r^2}{c^2}\frac{\partial k_{\max}}{\partial u} - 2\frac{\mathbf{r}_u \cdot \mathbf{n} + \mathbf{r} \cdot \mathbf{n}_u}{c^2}.$$

In a small vicinity of non-umbilical point P of $\mathbf{r}$, let us consider the lines of curvature parameterized by their arc lengths. Then the surface is locally represented in parametric form $\mathbf{r} = \mathbf{r}(u, v)$ for which

$$\mathbf{r}_u = \mathbf{t}_{\max}, \qquad \mathbf{r}_v = \mathbf{t}_{\min},$$

and the Rodrigues'curvature formula (see, for instance, [22, p. 94]) gives

$$\mathbf{n}_u = -k_{\max}\mathbf{t}_{\max}, \qquad \mathbf{n}_v = -k_{\min}\mathbf{t}_{\min}.$$

Now differentiating $\tilde{k}_{\max}$ and $\tilde{k}_{\min}$ in (7) and (8) along the *non*-corresponding curvature lines of $\mathbf{r}$ gives

$$\begin{aligned}\frac{\partial \tilde{k}_{\max}}{\partial v} &= \frac{\partial \tilde{k}_{\max}}{\partial \mathbf{t}_{\min}} = -2\frac{r}{c^2}\frac{\mathbf{t}_{\min} \cdot \mathbf{r}}{r} k_{\min} - \frac{r^2}{c^2} e_{\min} + \\ &\quad -2\frac{\mathbf{t}_{\min} \cdot \mathbf{n} - k_{\min}\mathbf{t}_{\min} \cdot \mathbf{r}}{c^2} = -\frac{r^2}{c^2} e_{\min},\end{aligned}$$

where $\mathbf{t}_{\min} \cdot \mathbf{n} = 0$ (because the principal directions live in the tangent plane of $\mathbf{r}$) and similar computations give us $\frac{\partial \tilde{k}_{\min}}{\partial u}$:

$$\frac{\partial \tilde{k}_{\max}}{\partial v} = -\frac{r^2}{c^2} e_{\min}, \qquad \frac{\partial \tilde{k}_{\min}}{\partial u} = -\frac{r^2}{c^2} e_{\max}. \tag{9}$$

Now let us denote by $\tilde{u}$ and $\tilde{v}$ the arclength parameterizations of the $\tilde{k}_{\max}$ and $\tilde{k}_{\min}$ curvature lines of $\tilde{\mathbf{r}}$, respectively, in a small vicinity of point $\tilde{P} \in \tilde{\mathbf{r}}$, the inversion image of $P \in \mathbf{r}$. Then, according to the first formula of (6), we have

$$d\tilde{u} = c^2 dv / r^2, \qquad d\tilde{v} = c^2 du / r^2. \tag{10}$$

In view of (9) and (10), we have

$$\begin{aligned}\frac{\partial \tilde{k}_{\max}}{\partial \tilde{\mathbf{t}}_{\max}} &= \frac{\partial \tilde{k}_{\max}}{\partial \tilde{u}} = \frac{\partial v}{\partial \tilde{u}} \frac{\partial \tilde{k}_{\max}}{\partial v} = \frac{r^2}{c^2}(-\frac{r^2}{c^2} e_{\min}), \\ \frac{\partial \tilde{k}_{\min}}{\partial \tilde{\mathbf{t}}_{\min}} &= \frac{\partial \tilde{k}_{\min}}{\partial \tilde{v}} = \frac{\partial u}{\partial \tilde{v}} \frac{\partial \tilde{k}_{\min}}{\partial u} = \frac{r^2}{c^2}(-\frac{r^2}{c^2} e_{\max}).\end{aligned}$$

Consequently, the curvature derivatives $\tilde{e}_{\max} = \partial \tilde{k}_{\max} / \partial \tilde{\mathbf{t}}_{\max}$ and $\tilde{e}_{\min} = \partial \tilde{k}_{\min} / \partial \tilde{\mathbf{t}}_{\min}$ relate to $e_{\max}$ and $e_{\min}$ by the following equations:

$$\frac{c^2}{r^2}\tilde{e}_{\max} = -\frac{r^2}{c^2} e_{\min}, \qquad \frac{c^2}{r^2}\tilde{e}_{\min} = -\frac{r^2}{c^2} e_{\max}. \tag{11}$$

Substituting (6) and (11) to (4) shows the inversion invariance property:

$$\iint \sqrt{\tilde{e}_{\max}^2 + \tilde{e}_{\min}^2} \, d\tilde{A} \;=\; \iint \sqrt{e_{\max}^2 + e_{\min}^2} \, dA.$$

It seems that the cross MVS energy (3) can not be modified such that it becomes inversion-invariant, since we have the terms depending on the principal directions of $\mathbf{r}$:

$$\begin{aligned}\frac{c^2}{r^2}\frac{\partial \tilde{k}_{\max}}{\partial \tilde{\mathbf{t}}_{\min}} &= -\frac{r^2}{c^2}\frac{\partial k_{\max}}{\partial \mathbf{t}_{\min}} + \frac{2}{c^2}(\mathbf{t}_{\max} \cdot \mathbf{r})(k_{\max} - k_{\min}), \\ \frac{c^2}{r^2}\frac{\partial \tilde{k}_{\min}}{\partial \tilde{\mathbf{t}}_{\max}} &= -\frac{r^2}{c^2}\frac{\partial k_{\min}}{\partial \mathbf{t}_{\max}} + \frac{2}{c^2}(\mathbf{t}_{\min} \cdot \mathbf{r})(k_{\min} - k_{\max}).\end{aligned}$$

3 Aesthetic Shapes and Curvature-based Creases

The CI-MVS energy (4) is closely related to the cyclides of Dupin and curvature-based surface creases. The cyclides were introduced by Dupin at the beginning of the 19th century, and have been studied in connection with various shape modeling tasks. See [4] for a historical survey and [6] for recent applications of the cyclides in geometric modeling as a CAGD primitive. The family of cyclides includes spheres, cylinders, cones, and tori.

Mathematically, the cyclides are characterized by the condition $e_{\max} = 0 = e_{\min}$, and obviously they are the best possible aesthetic shapes in terms of the MVS (2) and CI-MVS (4) energies. This can be interpreted by a concept of surface creases, the curves on a surface along which the surface bends sharply, described via extrema of $e_{\max}$ and $e_{\min}$:

$$e_{\max} = 0, \;\; \frac{\partial e_{\max}}{\partial \mathbf{t}_{\max}} < 0 \;\text{ and }\; e_{\min} = 0, \;\; \frac{\partial e_{\min}}{\partial \mathbf{t}_{\min}} > 0.$$

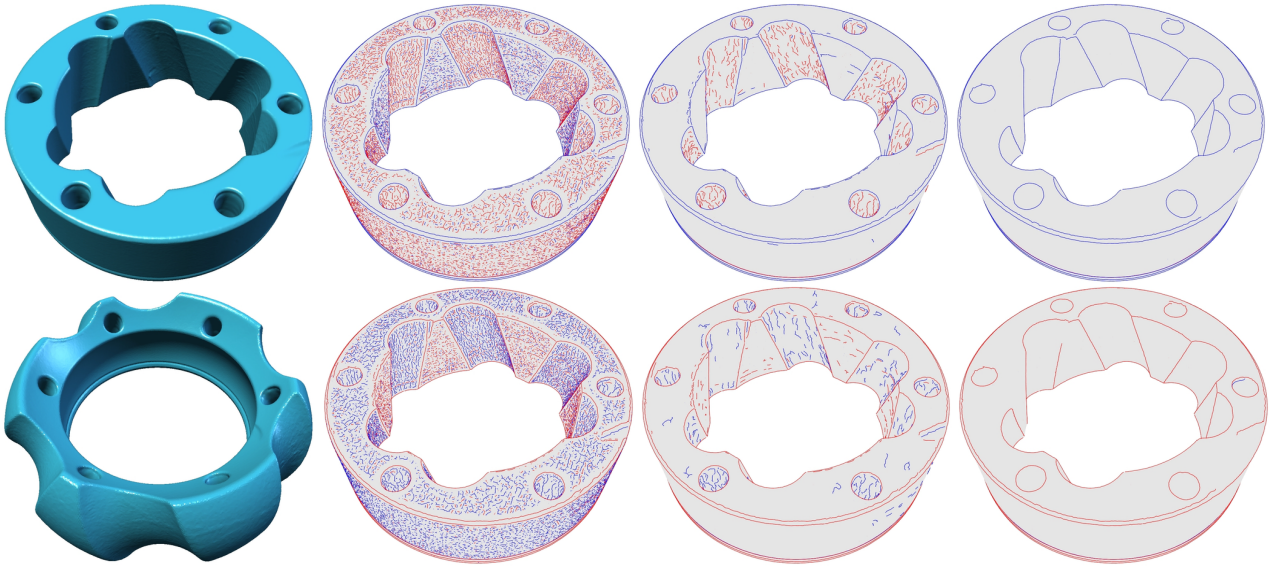

$\mathbf{r}$ (top) and $\tilde{\mathbf{r}}$ with $c = 1.0$ (bottom) $T \geq 0.0$ $T \geq 0.302$ $T \geq 7.3$

$F = 1.53\text{M}$, $s_{\mathbf{r}} = 4.795$, $E_B(\mathbf{r}) = 2904$, $E_M(\mathbf{r}) = 1.812 \times 10^7$, $E_C(\mathbf{r}) = 4320$,
$s_{\tilde{\mathbf{r}}} = 3.12$, $E_B(\tilde{\mathbf{r}}) = 2906$, $E_M(\tilde{\mathbf{r}}) = 9.444 \times 10^6$, and $E_C(\tilde{\mathbf{r}}) = 4321$.

Figure 2: The images demonstrate how well our thresholding scheme of (14) eliminates the unessential features of inversion dual crest lines.

Such curvature extremum curves, also called ridges-ravines and crest lines, have been employed in quality control of free-form surfaces [11] and also have numerous science and engineering applications (see [32] and references therein). It is interesting to mention that the ridge points and cyclides processes zero values for $e_{\max}$ and $e_{\min}$ but the cyclides do not have any creases since their second curvature derivatives of the cyclides are also zero everywhere $\partial e_{\max}/\partial \mathbf{t}_{\max} = 0 = \partial e_{\min}/\partial \mathbf{t}_{\min}$. This implies that the best aesthetic shapes in terms of a family of MVS energies consist of a set of cyclide patches whose boundaries become a set of ridges representing shape features. Similar concept has been employed for aesthetic shape modeling from feature lines [19, 20].

By (5) and (11), the ridges and cyclides are invariant under the conformal transformations. Therefore the conformal invariance property of aesthetic surfaces minimizing the variation of curvatures is also preferable. Consequently, our CI-MVS energy (4) has advantages over the traditional MVS energy (2).

Using (5) and (11) we arrive at

$$e^{\alpha}_{\max} ds^2_{\alpha} = e_{\max} ds^2 = -\tilde{e}_{\min} d\tilde{s}^2, \qquad (12)$$

$$e^{\alpha}_{\min} ds^2_{\alpha} = e_{\min} ds^2 = -\tilde{e}_{\max} d\tilde{s}^2 \qquad (13)$$

and can easily construct a number of conformal-invariant differential forms [32] (in principle, they can be derived from a complete conformal-invariant system derived in [23]). For example, a conformally invariant curve energy on a surface

$$T = \int \sqrt{|e_{\max}| + |e_{\min}|}\, ds \qquad (14)$$

is useful for filtering the unessential curvature extremum curves detected on a surface by eliminating the curves whose (14) are smaller than a given threshold value. Since (14) measures deviation from the cyclides, the remaining curves are more salient than the traditional curvature extremum curves. In addition, the above filtering scheme improves noise-robustness significantly when we use (14) for a detection of the curvature extremum curves on a mesh approximating a smooth surface, see Figure 2.

Equations (12) and (13) also lead to some interesting relations between scale and inversion transformations and curvature derivatives. For example, the rate of change of area by the scale and inversion transformations are inversely proportional to a ratio of the curvature derivatives:

$$\frac{\partial \tilde{A}}{\partial A} = -\frac{e_{\min}}{\tilde{e}_{\max}} = -\frac{e_{\max}}{\tilde{e}_{\min}}, \quad \frac{\partial A_{\alpha}}{\partial A} = \frac{e_{\max}}{e^{\alpha}_{\max}} = \frac{e_{\min}}{e^{\alpha}_{\min}},$$

$$\frac{e^{\alpha}_{\max}}{e^{\alpha}_{\min}} = \frac{e_{\max}}{e_{\min}} = \frac{\tilde{e}_{\min}}{\tilde{e}_{\max}}.$$

4 Inversion Dual Crest Lines

The so-called crest lines are formed by the perceptually salient ridge points and consist of the surface points where

the magnitude of the largest (in absolute value) principal curvature attains a maximum along its corresponding line of curvature [17]:

$$k_{\max} > |k_{\min}|, \qquad e_{\max} = 0, \qquad \frac{\partial e_{\max}}{\partial \mathbf{t}_{\max}} < 0,$$

$$k_{\min} < -|k_{\max}|, \qquad e_{\min} = 0, \qquad \frac{\partial e_{\min}}{\partial \mathbf{t}_{\min}} > 0.$$

The subset of crest lines of $\mathbf{r}$ such that

$$k_{\max} > |k_{\min}|, \tilde{k}_{\min} < -|\tilde{k}_{\max}|, e_{\max} = 0, \frac{\partial e_{\max}}{\partial \mathbf{t}_{\max}} < 0,$$

$$k_{\min} < -|k_{\max}|, \tilde{k}_{\max} > |\tilde{k}_{\min}|, e_{\min} = 0, \frac{\partial e_{\min}}{\partial \mathbf{t}_{\min}} > 0$$

are dual to the subset of crest lines of $\tilde{\mathbf{r}}$ such that

$$\tilde{k}_{\min} < -|\tilde{k}_{\max}|, k_{\max} > |k_{\min}|, \tilde{e}_{\min} = 0, \frac{\partial \tilde{e}_{\min}}{\partial \tilde{\mathbf{t}}_{\min}} > 0,$$

$$\tilde{k}_{\max} > |\tilde{k}_{\min}|, k_{\min} < -|k_{\max}|, \tilde{e}_{\max} = 0, \frac{\partial \tilde{e}_{\max}}{\partial \tilde{\mathbf{t}}_{\max}} < 0.$$

Note that the concave condition of $\tilde{\mathbf{r}}$ for the convex condition of $\mathbf{r}$, and vice versa is considered.

5 Numerical Experiments

In Figures 2-6, we examined our energies (4) and (14) and dual crest lines on several surfaces approximated by the triangle meshes, where F is a number of triangles (M: Mega), and $s_{\mathbf{r}}$ and $s_{\tilde{\mathbf{r}}}$ are the sizes of $\mathbf{r}$ and $\tilde{\mathbf{r}}$ (i.e. diagonal length of bounding box), respectively. The differential quantities on the triangle meshes are approximated by using the method in [32].

Figures 3-5 show differences between the traditional and inversion dual crest lines. The dual crest lines of $\tilde{\mathbf{r}}$ are calculated on $\tilde{\mathbf{r}}$ and then mapped onto $\mathbf{r}$ for visualization purpose. We obtain remarkably similar patterns for the inversion dual crest lines (see the bottom images of Figure 4 and (c,d) of Figure 5). Figures 2 and 6 demonstrate how well (14) eliminates the unessential creases located on the parts close to the cyclides.

Let $E_B(\cdot)$, $E_M(\cdot)$, and $E_C(\cdot)$ be the Willmore (1), MVS (2), and CI-MVS (4) energies. The $E_B(\cdot)$ and $E_C(\cdot)$ are numerically well preserved under spherical inversions compared with $E_M(\cdot)$ according to our numerical experiments. Our CI-MVS is much useful for evaluating surface quality compared with the other energies in terms of invariance property and shape aesthetics, although it is computationally expensive than others.

We have also compared CI-MVS (4) energy introduced in this paper with the scale-invariant MVS (SI-MVS) [19, 12]

$$\iint (e_{\max}^2 + e_{\min}^2)\, dA \cdot \iint dA \tag{15}$$

energy denoted by $E_S(\cdot)$ under spherical inversions in Figure 7. Numerical experiments suggest that CI-MVS is better than the SI-MVS in terms of Möbius invariance property as expected from our theoretical analysis.

6 Conclusion

The paper introduces a novel surface energy (CI-MVS energy) by modifying the minimum variation energy in order to satisfy invariance under conformal transformations. The CI-MVS energy consists of the principal curvatures and their first order derivatives w.r.t. corresponding principal directions, measures deviation from the cyclides, and provides better invariance properties than the conventional energy. We also studied connections of the CI-MVS with the cyclides and curvature extremum curves from a view of aesthetic shape design. In addition, we show how filtering with a conformally invariant curve energy on a surface improves a detection of the salient surface creases. Future work will aim at developing numerical methods for minimizing the CI-MVS efficiently for the given initial and boundary conditions.

Acknowledgements. This work was supported in part by Grants-in-Aid for Scientific Research of Japan (24700182 and 20113007). The models are courtesy of AIM@SHAPE shape repository (Camel, Caesar, Gargoyle, Gearbox, Pegasos, and Rolling Stage), FarField Technology Ltd (Hand), INRIA (Car), MPI Informatik (Max-Planck bust), MIT Computer Graphics Group (Elephant and Horse), Stanford University (Armadillo, Bunny, and Dragon), and University of Washington (Fandisk).

References

[1] B. BASTL, B. JÜTTLER, M. LÁVIČKA, AND Z. ŠÍR, *Curves and surfaces with rational chord length parameterization*, Computer Aided Geometric Design, 29 (2012), pp. 231–241.

[2] A. I. BOBENKO AND P. SCHRÖDER, *Discrete Willmore flow*, in Eurographics Symposium on Geometry Processing, 2005, pp. 101–110.

[3] C. BOHLE, G. P. PETERS, AND U. PINKALL, *Constrained willmore surfaces*, Calculus of Variations and Partial Differential Equations, 32 (2008), pp. 263–277.

[4] V. CHANDRU, D. DUTTA, AND C. M. HOFFMANN, *On the geometry of Dupin cyclides*, The Visual Computer, 5 (1989), pp. 277–290.

[5] L. EULER, *Additamentum 'de curvis elasticis'*, in Methodus Inveniendi Lineas Curvas Maximi Minimive Probprietate Gaudentes, Lausanne, 1744.

[6] S. FOUFOU AND L. GARNIER, *Dupin cyclide blends between quadric surfaces for shape modeling*, Computer Graphics Forum, 23 (2004), pp. 321–330. Proc. of Eurographics.

[7] J. GRAVESEN AND M. UPGSTRUP, *Constructing invariant fairness measures for surfaces*, Advances in Computational Mathematics, 17 (2002), pp. 67–88.

[8] X. GU AND S.-T. YAU, *Surface classification using conformal structures*, in Proceedings of IEEE International Conference on Computer Vision, IEEE Computer Society, 2003, pp. 701–708.

[9] J. GUVEN, *Conformally invariant bending energy for hypersurfaces*, Journal of Physics A: Mathematical and General, 38 (2005), pp. 7943–7956.

[10] U. HERTRICH-JEROMIN, *Introduction to Möbius Differential Geometry*, Cambridge University Press, 2003.

[11] M. HOSAKA, *Modeling of Curves and Surfaces in CAD/CAM*, Springer, Berlin, 1992.

[12] P. JOSHI AND C. SÉQUIN, *Energy minimizers for curvature-based surface functionals*, Computer-Aided Design and Applications, 4 (2007), pp. 607–618.

[13] R. LEVIEN, *The elastica: a mathematical history*, Tech. Rep. UCB/EECS-2008-103, EECS Department, University of California, Berkeley, 2008.

[14] S. MANN AND L. DORST, *Geometric algebra: a computational framework for geometrical applications, part 2*, IEEE Computer Graphics and Applications, 22 (2002), pp. 58–67.

[15] F. C. MARQUES AND A. NEVES, *Min-max theory and the Willmore conjecture*, http://arxiv.org/abs/1202.6036, 2012.

[16] R. MEHRA, P. TRIPATHI, A. SHEFFER, AND N. J. MITRA, *Visibility of noisy point cloud data*, Computers and Graphics, 34 (2010), pp. 219–230. SMI'10.

[17] O. MONGA, S. BENAYOUN, AND O. D. FAUGERAS, *From partial derivatives of 3-d density images to ridge lines*, in Proceedings of IEEE Conference on Computer Vision and Pattern Recognition, IEEE Computer Society, 1992, pp. 354 – 359.

[18] H. P. MORETON AND C. H. SÉQUIN, *Surface design with minimum energy networks*, in Proceedings of ACM Symposium on Solid Modeling Foundations and CAD/CAM Applications, ACM, 1991, pp. 291–301.

[19] H. P. MORETON AND C. H. SÉQUIN, *Functional optimization for fair surface design*, in Proceedings of ACM SIGGRAPH, 1992, pp. 167–176.

[20] A. NEALEN, T. IGARASHI, O. SORKINE, AND M. ALEXA, *Fibermesh: designing freeform surfaces with 3d curves*, ACM Transactions on Graphics, 26 (2007), pp. 41:1–10. Proc. of ACM SIGGRAPH.

[21] T. RIVIÉRE, *Analysis aspects of willmore surfaces*, Inventiones Mathematicae, 174 (2008), pp. 1–45.

[22] D. J. STRUIK, *Lectures on Classical Differential Geometry: Second Edition*, Dover Publications, Inc. New York, 1988.

[23] C. P. WANG, *Surfaces in Möbius geometry*, Nagoya Mathematical Journal, 125 (1992), pp. 53–72.

[24] M. WARDETZKY, M. BERGOU, D. HARMON, D. ZORIN, AND E. GRINSPUN, *Discrete quadratic curvature energies*, Computer Aided Geometric Design, 24 (2007), pp. 499–518.

[25] R. WAREHAM, J. CAMERON, AND J. LASENBY, *Applications of conformal geometric algebra in computer vision and graphics*, in Proceedings of International Conference on Computer Algebra and Geometric Algebra with Applications, Springer-Verlag, 2005, pp. 329–349.

[26] C. E. WEATHERBURN, *Differential Geometry of Three Dimensions, volume I*, Cambridge University Press, 1927.

[27] J. H. WHITE, *A global invariant of conformal mappings in space*, Proceedings of the American Mathematical Society, 38 (1973), pp. 162–164.

[28] T. J. WILLMORE, *Note on embedded surfaces*, Anal. Stunt. Ale Univ. Sect. I. a Math., 11B (1965), pp. 493–496.

[29] T. J. WILLMORE, *Surfaces in conformal geometry*, Annals of Global Analysis and Geometry, 18 (2000), pp. 255–264.

[30] G. XU AND Q. ZHANG, *Minimal mean-curvature-variation surfaces and their applications in surface modeling*, in Proceedings of International Conference on Geometric Modeling and Processing, Springer-Verlag, 2006, pp. 357–370.

[31] S. YOSHIZAWA AND A. BELYAEV, *Conformally invariant energies and minimum variation surfaces*, in Proceedings of Asian Conference on Design and Digital Engineering, Niseko, Hokkaido, Japan, December 2012.

[32] S. YOSHIZAWA, A. BELYAEV, H. YOKOTA, AND H.-P. SEIDEL, *Fast, robust, and faithful methods for detecting crest lines on meshes*, Computer Aided Geometric Design, 25 (2008), pp. 545–560.

Appendix A. Sphere Inversions and Surface Curvatures. Given a surface $\mathbf{r} = \mathbf{r}(u, v)$, consider its spherical inversion with radius c w.r.t. the origin of coordinates

$$\tilde{\mathbf{r}} = \tilde{\mathbf{r}}(u, v) = \frac{c^2}{r^2(u, v)}\mathbf{r}(u, v),$$

where $r^2 = r^2(u, v) = \mathbf{r} \cdot \mathbf{r}$. Since $\frac{\partial(\mathbf{r}\cdot\mathbf{r})}{\partial u} = 2\mathbf{r}_u \cdot \mathbf{r} = 2\frac{\partial r}{\partial u}r = 2r_u r$ and $\frac{\partial(\mathbf{r}\cdot\mathbf{r})}{\partial v} = 2\mathbf{r}_v \cdot \mathbf{r} = 2\frac{\partial r}{\partial v}r = 2r_v r$, we have $r_u = \frac{\mathbf{r}_u\cdot\mathbf{r}}{r}$ and $r_v = \frac{\mathbf{r}_v\cdot\mathbf{r}}{r}$ such that the basic tangents of $\tilde{\mathbf{r}}$ are given by differentiating $\tilde{\mathbf{r}}$ w.r.t. u and v:

$$\frac{\partial\tilde{\mathbf{r}}}{\partial u} = \tilde{\mathbf{r}}_u = -2\frac{c^2}{r^4}(\mathbf{r}_u \cdot \mathbf{r})\mathbf{r} + \frac{c^2}{r^2}\mathbf{r}_u, \qquad (16)$$

$$\frac{\partial\tilde{\mathbf{r}}}{\partial v} = \tilde{\mathbf{r}}_v = -2\frac{c^2}{r^4}(\mathbf{r}_v \cdot \mathbf{r})\mathbf{r} + \frac{c^2}{r^2}\mathbf{r}_v \qquad (17)$$

where $\mathbf{r}_u = \frac{\partial\mathbf{r}}{\partial u}$ and $\mathbf{r}_v = \frac{\partial\mathbf{r}}{\partial v}$ are the basic tangents of $\mathbf{r}$. Then, their inner products give the coefficients of the first fundamental form of $\tilde{\mathbf{r}}$:

$$\tilde{E} = \tilde{\mathbf{r}}_u^2 = \frac{c^4}{r^4}E, \quad \tilde{F} = \tilde{\mathbf{r}}_u \cdot \tilde{\mathbf{r}}_v = \frac{c^4}{r^4}F, \quad \tilde{G} = \tilde{\mathbf{r}}_v^2 = \frac{c^4}{r^4}G,$$

where $E = \mathbf{r}_u^2$, $F = \mathbf{r}_u \cdot \mathbf{r}_v$, and $G = \mathbf{r}_v^2$ are the coefficients of the first fundamental form of $\mathbf{r}$. Thus, the area element of $\tilde{\mathbf{r}}$ is given by

$$\iint d\tilde{A} = \iint \sqrt{\tilde{E}\tilde{G} - \tilde{F}^2}\, dudv = \iint \frac{c^4}{r^4}dA,$$

where $dA = \sqrt{EG - F^2}\, dudv$ is the area element of $\mathbf{r}$.

Let $\mathbf{n}$ be the unit normal vector of $\mathbf{r}$. The unit normal vector of $\tilde{\mathbf{r}}$ is given by

$$\tilde{\mathbf{n}} = \frac{\tilde{\mathbf{r}}_u \times \tilde{\mathbf{r}}_v}{\sqrt{\tilde{E}\tilde{G} - \tilde{F}^2}} = -\frac{2}{r^2}((\mathbf{r}_v \cdot \mathbf{r})\mathbf{r}_u - (\mathbf{r}_u \cdot \mathbf{r})\mathbf{r}_v) \times \mathbf{r} + \mathbf{n},$$

By using the formulas of vector triple product:

$$\mathbf{a}\times(\mathbf{b}\times\mathbf{c}) = (\mathbf{a}\cdot\mathbf{c})\mathbf{b} - (\mathbf{a}\cdot\mathbf{b})\mathbf{c}, (\mathbf{a}\times\mathbf{b})\times\mathbf{c} = (\mathbf{c}\cdot\mathbf{a})\mathbf{b} - (\mathbf{c}\cdot\mathbf{b})\mathbf{a},$$

we obtain

$$\tilde{\mathbf{n}} = -\frac{2}{r^2}(\mathbf{r} \times \mathbf{n}) \times \mathbf{r} + \mathbf{n} = \frac{2}{r^2}(\mathbf{r} \cdot \mathbf{n})\mathbf{r} - \mathbf{n}.$$

Differentiating (16) and (17), and their inner products with $\tilde{\mathbf{n}}$ lead the coefficients of the second fundamental form of $\tilde{\mathbf{r}}$:

$$\begin{aligned}\tilde{L} &= \tilde{\mathbf{r}}_{uu} \cdot \tilde{\mathbf{n}} = (8\frac{c^2}{r^6}(\mathbf{r}_u \cdot \mathbf{r})^2\mathbf{r} - 2\frac{c^2}{r^4}(\mathbf{r}_{uu} \cdot \mathbf{r} + E)\mathbf{r} + \\ &\quad -4\frac{c^2}{r^4}(\mathbf{r}_u \cdot \mathbf{r})\mathbf{r}_u + \frac{c^2}{r^2}\mathbf{r}_{uu}) \cdot (\frac{2}{r^2}(\mathbf{r} \cdot \mathbf{n})\mathbf{r} - \mathbf{n}) \\ &= -\frac{c^2}{r^2}(L + \frac{2}{r^2}(\mathbf{r} \cdot \mathbf{n})E),\end{aligned}$$

and similar computations give us

$$\begin{aligned}\tilde{M} &= \tilde{\mathbf{r}}_{uv} \cdot \tilde{\mathbf{n}} = -\frac{c^2}{r^2}(M + \frac{2}{r^2}(\mathbf{r} \cdot \mathbf{n})F), \\ \tilde{N} &= \tilde{\mathbf{r}}_{vv} \cdot \tilde{\mathbf{n}} = -\frac{c^2}{r^2}(N + \frac{2}{r^2}(\mathbf{r} \cdot \mathbf{n})G),\end{aligned}$$

where $L = \mathbf{r}_{uu} \cdot \mathbf{n}$, $M = \mathbf{r}_{uv} \cdot \mathbf{n}$, and $N = \mathbf{r}_{vv} \cdot \mathbf{n}$ are the coefficients of the second fundamental form of $\mathbf{r}$.

Substitute the above results into the following formulas of the mean and Gaussian curvatures

$$\begin{aligned}\tilde{H} &= \frac{1}{2}\frac{\tilde{E}\tilde{N} - 2\tilde{F}\tilde{M} + \tilde{G}\tilde{L}}{\tilde{E}\tilde{G} - \tilde{F}^2} = -\frac{r^2}{c^2}H - 2\frac{(\mathbf{r} \cdot \mathbf{n})}{c^2}, \\ \tilde{K} &= \frac{\tilde{L}\tilde{N} - \tilde{M}^2}{\tilde{E}\tilde{G} - \tilde{F}^2} = \frac{r^4}{c^4}K + 4\frac{r^2}{c^4}(\mathbf{r} \cdot \mathbf{n})H + 4\frac{(\mathbf{r} \cdot \mathbf{n})^2}{c^4}\end{aligned}$$

where $H = \frac{1}{2}\frac{EN-2FM+GL}{EG-F^2}$ and $K = \frac{LN-M^2}{EG-F^2}$ are the mean and Gaussian curvatures of $\mathbf{r}$, respectively. Let $\tilde{k}_{\max}$ and $\tilde{k}_{\min}$ be the principal curvatures of $\tilde{\mathbf{r}}$ and then substitute the above equations in $\tilde{H} = (\tilde{k}_{\max} + \tilde{k}_{\min})/2$, $\tilde{K} = \tilde{k}_{\max}\tilde{k}_{\min}$, $\tilde{k}_{\max} = \tilde{H} + \sqrt{\tilde{H}^2 - \tilde{K}}$, and $\tilde{k}_{\min} = \tilde{H} - \sqrt{\tilde{H}^2 - \tilde{K}}$ with $k_{\max} \geq k_{\min}$, $c^2 > 0$, and $r^2 \geq 0$ gives

$$\begin{aligned}\tilde{k}_{\max} &= -\frac{r^2}{c^2}k_{\min} - 2\frac{(\mathbf{r} \cdot \mathbf{n})}{c^2}, \\ \tilde{k}_{\min} &= -\frac{r^2}{c^2}k_{\max} - 2\frac{(\mathbf{r} \cdot \mathbf{n})}{c^2}\end{aligned}$$

where $k_{\max}$ and $k_{\min}$ are the principal curvatures of $\mathbf{r}$.

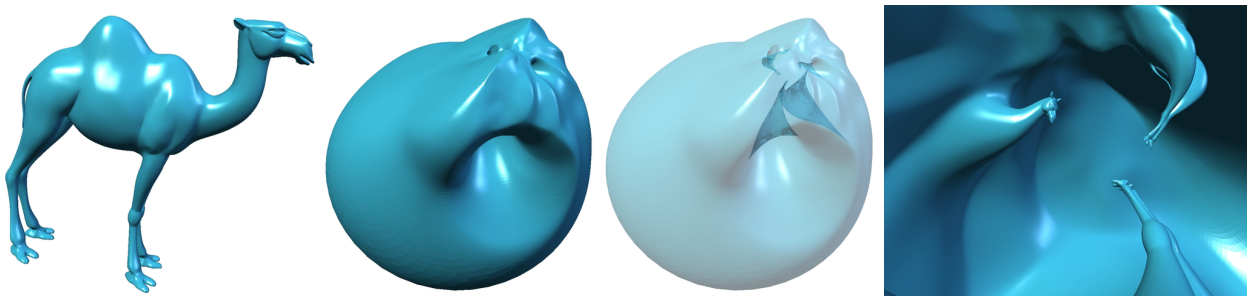

(a) (b) (c)

Figure 3: (a): Input mesh $\mathbf{r}$. (b): Transformed mesh $\tilde{\mathbf{r}}$ with $c = 0.1$. (c): Magnified image of (b). $F = 1.25$M, $s_{\mathbf{r}} = 2.031$, $E_B(\mathbf{r}) = 8449$, $E_M(\mathbf{r}) = 8.1262 \times 10^{12}$, $E_C(\mathbf{r}) = 12585$, $s_{\tilde{\mathbf{r}}} = 0.5$, $E_B(\tilde{\mathbf{r}}) = 8468$, $E_M(\tilde{\mathbf{r}}) = 3.3567 \times 10^{16}$, and $E_C(\tilde{\mathbf{r}}) = 12605$. The difference between $E_C(\mathbf{r})$ and $E_C(\tilde{\mathbf{r}})$ is very small compared with the MVS energy difference ($E_M(\mathbf{r})$ and $E_M(\tilde{\mathbf{r}})$).

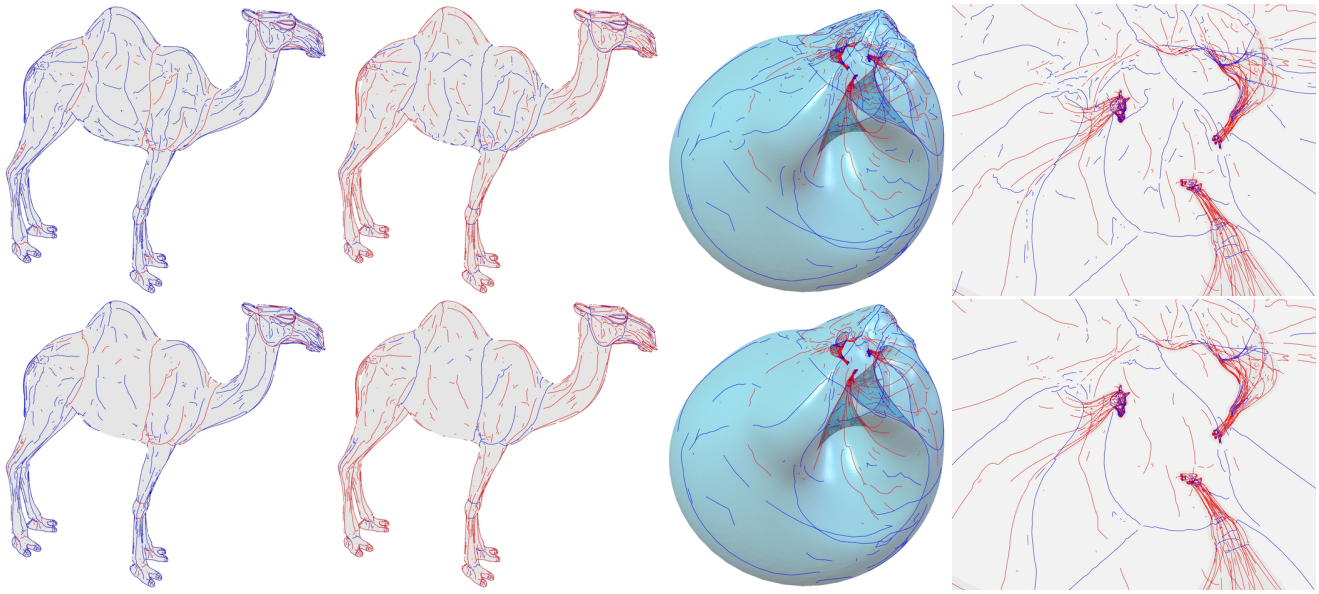

(a) (b) (c) (d)

Figure 4: The top (bottom) images (a) and (b,c,d) present the crest lines (inversion dual crest lines) of $\mathbf{r}$ and $\tilde{\mathbf{r}}$, respectively, where the input meshes are shown in images (a) and (b,c) of Figure 3. The traditional crest lines (top images) of $\mathbf{r}$ and $\tilde{\mathbf{r}}$ do not coincide when their convex and concave lines are exchanged, while the inversion dual crest lines (bottom images) share common geometric patterns.

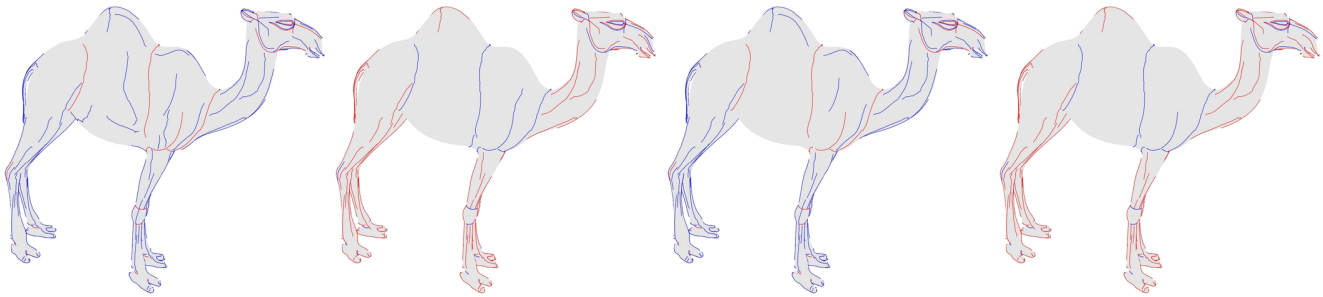

(a) (b) (c) (d)

Figure 5: Filtered crest lines (inversion dual crest lines) are demonstrated in (a) and (b) ((c) and (d)) whose threshold value (14) is greater than 1.5. Images (a,b) and (c,d) correspond to top and bottom images of Figure 4, respectively.

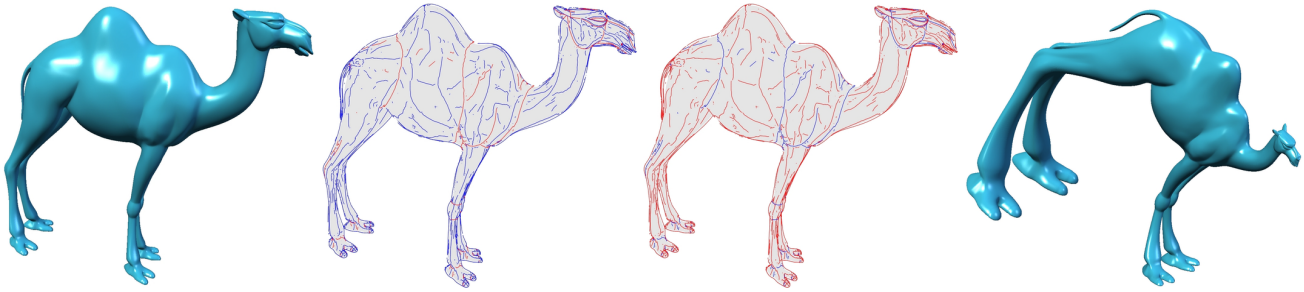

$c = 1.5$, $T \geq 0.0$, $s_{\tilde{\mathbf{r}}} = 1.658$, $E_B(\tilde{\mathbf{r}}) = 8453$, $E_M(\tilde{\mathbf{r}}) = 1.0146 \times 10^{14}$, and $E_C(\tilde{\mathbf{r}}) = 12581$.

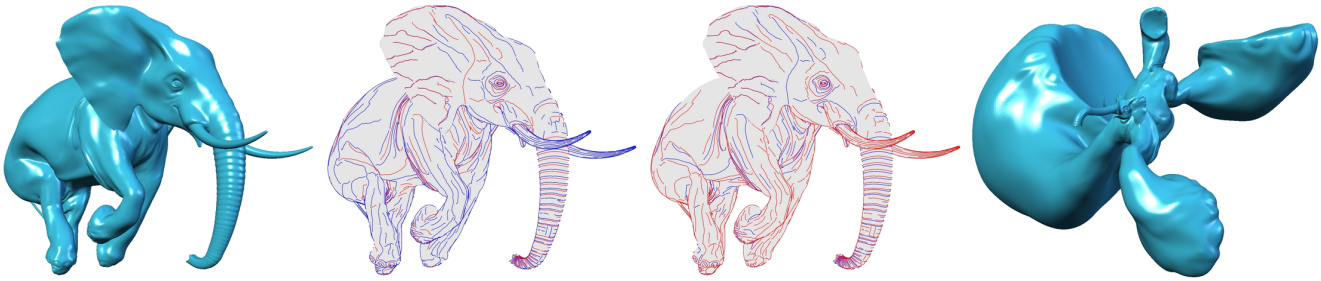

$c = 0.5$, $T \geq 0.5$, $F = 1.35$M, $s_{\mathbf{r}} = 1.609$, $E_B(\mathbf{r}) = 1.387 \times 10^5$, $E_M(\mathbf{r}) = 7.81 \times 10^{13}$, $E_C(\mathbf{r}) = 1.073 \times 10^5$,
$s_{\tilde{\mathbf{r}}} = 5.697$, $E_B(\tilde{\mathbf{r}}) = 1.382 \times 10^5$, $E_M(\tilde{\mathbf{r}}) = 7.857 \times 10^{14}$, and $E_C(\tilde{\mathbf{r}}) = 1.07 \times 10^5$.

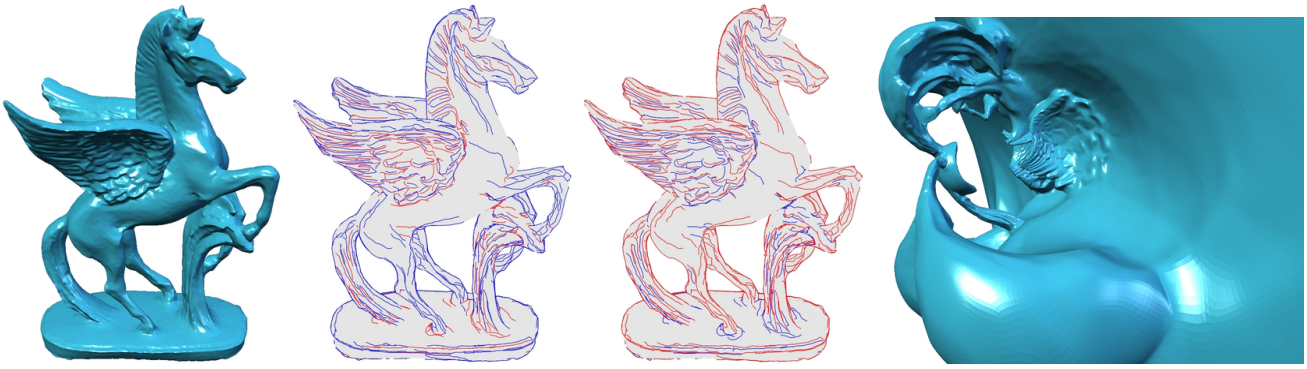

$c = 10.0$, $T \geq 2.0$, $F = 1.96$M, $s_{\mathbf{r}} = 200.2$, $E_B(\mathbf{r}) = 2.112 \times 10^4$, $E_M(\mathbf{r}) = 4.072 \times 10^8$, $E_C(\mathbf{r}) = 2.387 \times 10^4$,
$s_{\tilde{\mathbf{r}}} = 82.63$, $E_B(\tilde{\mathbf{r}}) = 2.118 \times 10^4$, $E_M(\tilde{\mathbf{r}}) = 1.046 \times 10^{12}$, and $E_C(\tilde{\mathbf{r}}) = 2.408 \times 10^4$.

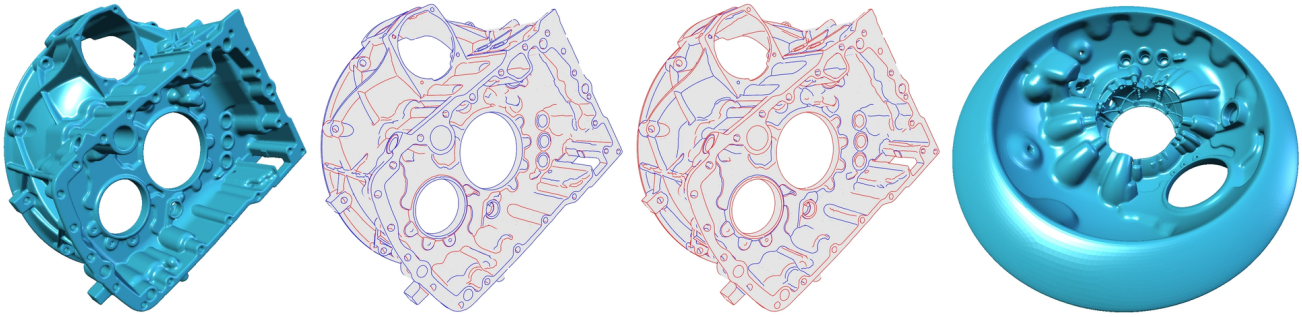

$c = 0.25$, $T \geq 2.0$, $F = 2.06$M, $s_{\mathbf{r}} = 1.483$, $E_B(\mathbf{r}) = 3.774 \times 10^4$, $E_M(\mathbf{r}) = 3.774 \times 10^4$, $E_C(\mathbf{r}) = 6.821 \times 10^4$,
$s_{\tilde{\mathbf{r}}} = 1.3$, $E_B(\tilde{\mathbf{r}}) = 3.775 \times 10^4$, $E_M(\tilde{\mathbf{r}}) = 4.78 \times 10^{10}$, and $E_C(\tilde{\mathbf{r}}) = 5.007 \times 10^4$.

(a) (b) (c) (d)

Figure 6: Images (b) and (c) show the inversion dual crest lines of (a) and (d) which correspond to $\mathbf{r}$ and $\tilde{\mathbf{r}}$, respectively. The mesh model shown in the top image is generated by translating the model of Figure 3. Remarkably similar feature patterns are extracted on (b) and (c), and we can confirm inversion duality of them as well as small differences between $E_C(\mathbf{r})$ and $E_C(\tilde{\mathbf{r}})$.

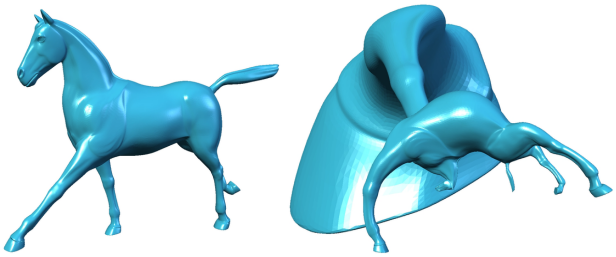

(a):$c = 1.0$, $F = 0.27$M.

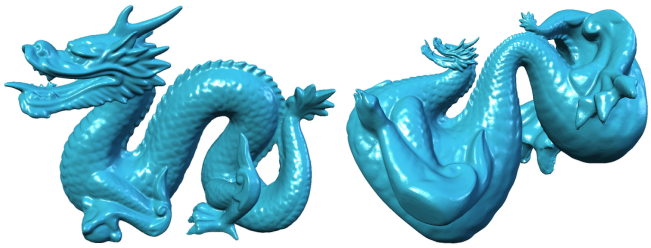

(b):$c = 0.1$, $F = 0.87$M.

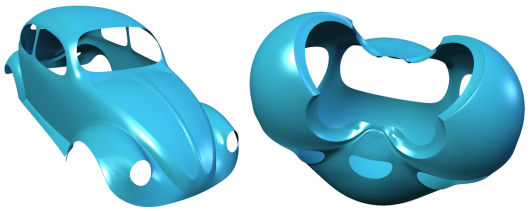

(c):$c = 0.5$, $F = 0.62$M.

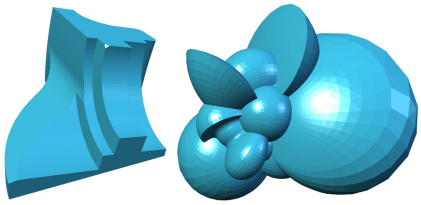

(d):$c = 2.0$, $F = 0.013$M.

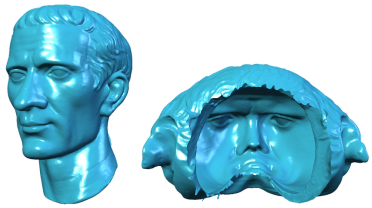

(e):$c = 100.0$, $F = 0.8$M.

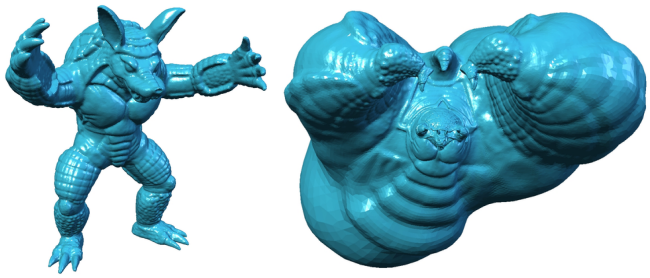

(f):$c = 10.0$, $F = 0.35$M.

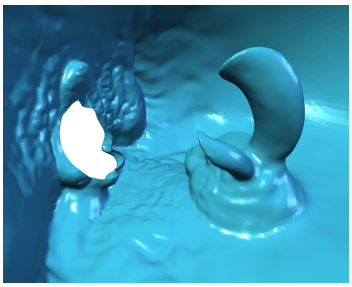

(g):$c = 2.0$, $F = 0.25$M.

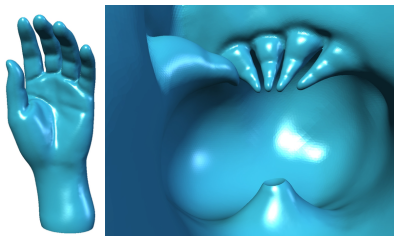

(h):$c = 20.0$, $F = 0.31$M.

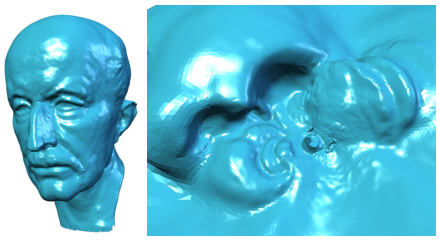

(i):$c = 20.0$, $F = 0.4$M.

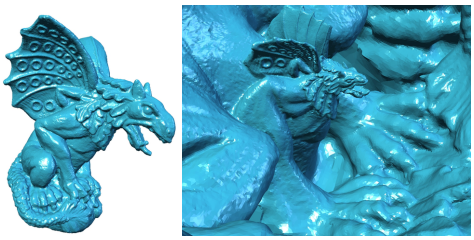

(j):$c = 100.0$, $F = 0.5$M.

	(a)	(b)	(c)	(d)	(e)
$E_S(\mathbf{r})$	5.26×10^{11}	1.5×10^{16}	3.13×10^{9}	2.14×10^{6}	1.0×10^{8}
$E_S(\tilde{\mathbf{r}})$	1.02×10^{14}	8.56×10^{16}	3.18×10^{10}	2.27×10^{7}	1.9×10^{9}
$E_C(\mathbf{r})$	1.02×10^{4}	2.12×10^{4}	1.49×10^{3}	7.68×10^{2}	5.04×10^{3}
$E_C(\tilde{\mathbf{r}})$	1.02×10^{4}	2.12×10^{4}	1.55×10^{3}	8.85×10^{2}	4.99×10^{3}
	(f)	(g)	(h)	(i)	(j)
$E_S(\mathbf{r})$	1.5×10^{9}	3.46×10^{7}	2.85×10^{10}	2.74×10^{8}	8.64×10^{11}
$E_S(\tilde{\mathbf{r}})$	1.02×10^{11}	7.86×10^{8}	1.86×10^{13}	8.32×10^{11}	2.17×10^{14}
$E_C(\mathbf{r})$	7.88×10^{3}	1.75×10^{3}	1.91×10^{3}	3.11×10^{3}	2.44×10^{4}
$E_C(\tilde{\mathbf{r}})$	7.93×10^{3}	1.81×10^{3}	2.06×10^{3}	3.36×10^{3}	2.23×10^{4}

Figure 7: The images (a-j) and their corresponding values demonstrate how well our CI-MVS (4) energy is preserved under spherical inversions compared with the SI-MVS (15) energy. Here the left and right images correspond to the input and transformed meshes via spherical inversions.